Discrete time model for chemical or biological decay in chaotic flows: Reentrance phase transitions

Izabella Júlia Benczik
Max Planck Institute for the Physics of Complex Systems, Nöthnitzer Strasse 38, 01187 Dresden, Germany and Department of Theoretical Physics, Eötvös University, H-1518 Budapest, Hungary
(Received 18 December 2004; published 15 June 2005)

We consider a discrete time model of advection, reaction, and diffusion on a lattice to investigate the steady-state spatial structure of chemically decaying substances. The time discretization of the dynamics has a considerable impact on these structures. Additional smooth-filamental phase transitions, nonexistent in the continuous-time description, appear. We show how these structures and their scaling properties depend on the time step of the discrete dynamics. Exploiting the analogies of this discrete model with the logistic map, some general features are discussed.

DOI: 10.1103/PhysRevE.71.066205 PACS number(s): 05.45.−a, 47.52.+j, 47.70.Fw, 47.53.+n

I. INTRODUCTION

Reactive flows play an important role in nature and technology, and they are ubiquitous in the atmosphere and the oceans. Stratospheric ozone chemistry is one of the most studied examples where complex interaction between transport processes and chemical reactions leads to the formation of the "ozone hole" in the polar regions of the stratosphere [1,2]. Biological population dynamics in a fluid environment can also be described within the framework of reactive flows. Phytoplankton is the primary producer of the aquatic ecosystem's food chain and plays a crucial role as a key ingredient in the carbon exchange process between the oceans and atmosphere and thus in regulating the greenhouse effect. The complex interaction of nutrients and plankton species in the upper layer of the ocean is influenced by the stirring due to mesoscale eddies [3,4]. The stirring process typically leads to the formation of complex filamental structures [5], which in observations (for example through remote sensing of satellite imaging) are clearly dominating the picture. These structures enhance chemical and biological activity in flows [6–9].

The general description of these reactive scalar fields (i.e., concentrations of reacting chemicals or interacting biological populations in a fluid) involves nonlinear differential equations. The dynamics is governed by the so-called advection-diffusion-reaction equations. However, some of the photochemical reactions in the atmosphere proceed only in the presence of light and stop by night [2], which makes the process discrete. Also, in some biological situations population growth or death processes can be modeled in discrete time intervals (for instance, in Ref. [10]). In the case of phytoplankton, factors such as the time that these photosynthesis-capable organisms spend exposed to solar light, or the periodic warming of the water, can discretize the processes in which the species are participating. In general, a discrete approach is reasonable whenever the occurrence of the reaction is determined by a periodic phenomenon (e.g., the daily cycle of the light) which has a characteristic time scale of the same order of magnitude as the species' lifetime (otherwise we can neglect its time dependence and use an average value in equations). The appropriate mathematical description in these cases is in terms of difference equations and iterative maps.

In this paper, we discuss the advection-diffusion-reaction problem in a time-discrete framework. The first work which defines discrete time evolution for reaction-advection systems is Ref. [9], virtually starting this research area. Similar problems, and the question itself of whether a given discrete process can be modeled in a continuous way in reactive dynamics, were discussed in Refs. [11,12]. In the second article, the authors modeled the reaction by a standard map and the population dynamics by a logistic map.

In the present work, the emphasis will be on the effects of time discretization on reactive patterns with respect to the ones appearing in the time continuous description. It was shown in Refs. [13,14] (regarding linearly decaying chemical substances in a time continuous context) that in chaotic flows the steady-state spatial distribution of the products for certain parameter is smooth while for others it might become filamental (nondifferentiable). We will show that in discrete time processes, new smooth-filamental transitions appear in the dynamics. The phenomenon is new, nonexistent in the continuous-time description, and it can contribute to a better understanding of the appearance of the filamental structures in such systems.

The paper is structured as follows. In Sec. II, we introduce the advection-reaction-diffusion problem investigated in the paper. In the next section, we present the flow model and the reaction, both of them in the sense of the lattice-mixing algorithm based on the discretization of the phase space. Section IV contains numerical evidence of smooth and filamental distributions appearing in the steady state, and an analytical description of the smooth-filamental transition (see also the Appendix) giving the exact condition for the transition in terms of the Hölder exponent. In Sec. V, the time continuous limit is discussed. In Sec. VI, we give a generalization of the findings to more general systems of biological relevance. Finally, in section VII the results are summarized along with mentioning possible further research topics.

II. THE MODEL

Earlier findings of Refs. [13,14], regarding the time continuous description of advection-reaction-diffusion systems, constitute a valuable basis for comparison with the discrete dynamics. For the sake of convenience, as a workbench system we use the same particular case of flow and reaction as in the mentioned works. The novel features, however, are the nonlinearity of the reaction (as justified below) and the generalization of the model to more realistic situations. We consider the simple case of a single substance advected by a time-dependent two-dimensional closed flow. The reactive evolution of a fluid element is taken in the form of an order γ chemical decay. In order to obtain a nontrivial concentration field at long times, we include a space-dependent source $S(\mathbf{r})$ of the substance. The concentration field in the time continuous description is governed by the partial differential equation

$$\frac{\partial C}{\partial t} + [\mathbf{u}(\mathbf{r},t)\cdot\boldsymbol{\nabla}]C = S(\mathbf{r}) - b\,C^{\gamma} + D\boldsymbol{\nabla}^2 C, \tag{1}$$

where b is the decay rate and $\mathbf{u}(\mathbf{r},t)$ is the known flow field. This linear ($\gamma=1$) or nonlinear ($\gamma\neq 1$) decay can be regarded as a simplified qualitative model for the decay of atmospheric pollutants. Similar processes are relevant in ozone photochemistry for the destruction of stratospheric ozone mediated by halogen compounds [2]. It can also describe decomposition of unstable radicals and relaxation of the sea surface temperature to mean values [15] ($\gamma=1$). For plankton dynamics, the exponent in the second term is usually taken either $\gamma=1$ or 2. The former case represents the exponential abiotical death or the sinking of the phytoplankton, while the latter is of biotical character due to the competition between individuals. The source term describes a localized and quantified input of the species in the mixing region, such as, for example, due to localized warming or upwellings of nutrient-rich water from deeper ocean layers. In the vegetation period (early summer), both the reproduction of the individuals (e.g., diatoms [16]) and their death due to competition ($\gamma=2$ decay) have a maximal intensity during day (the diatoms are in the upper layer of the ocean exposed to solar light) and a minimum point during night (the plankton is sinked). Since besides the above-mentioned chemical processes this problem of biological origin constitutes the other principal motivation for the present work, in the following by "reaction" we will mean not only chemical, but also biological activity.

Although real atmospheric or oceanic processes involve a large number of species and reactions, the simple model above captures the main characteristic features of these reactive systems, namely nonlinearity and a relaxational (stable) nonuniform equilibrium state.

III. DISCRETE TIME MODEL FOR ADVECTION-REACTION-DIFFUSION PROBLEMS

In order to take into account the discrete character of the processes, we model the reactive flow in numerical experiments by a discrete map both for mixing and reaction. The advection dynamics in a closed flow with periodic boundary conditions can be described by the *lattice mixing algorithm* proposed by Pierrehumbert [17]. The main idea is to replace the advection in the velocity field (u_x,u_y), by an area-preserving map's discrete iterations defined by

$$x_{n+1} = x_n + \left[\frac{u_x}{\Delta x}\tau\right]\Delta x,$$

$$y_{n+1} = y_n + \left[\frac{u_y}{\Delta y}\tau\right]\Delta y, \tag{2}$$

which maps the fluid particles from their initial positions $\mathbf{r}_n=(x_n,y_n)$ assumed to be on a discrete, Cartesian, $N\times N$ lattice of linear size unity, to their advected position $\mathbf{r}_{n+1}=(x_{n+1},y_{n+1})$ at some time lag τ later. The integer value $[*]$ assures that the points are translated under the map with multiple integers of the lattice spacings $\Delta x=1/N$ and $\Delta y=1/N$, respectively.

For numerical investigations, we take a simple standard model of a time-periodic flow [19] that consists of the alternation of two steady sinusoidal shear flows,

$$u_x = A_0\cos(2\pi y_n),$$

$$u_y = 0, \tag{3}$$

in the x direction and

$$u_x = 0,$$

$$u_y = A_0\cos(2\pi x_n), \tag{4}$$

in the y direction for the first and the second half of the period, respectively. The parameter A_0 controls the chaotic behavior of the flow. We choose the value $A_0=2.4$ which produces a flow with a single connected chaotic region without visible KAM tori. The period of the flow T is taken to be the time unit. On an $N\times N$ Cartesian lattice, map (2) is defined on the unit square with periodic boundary conditions,

$$x_{n+1} = x_n + [A_0\cos(2\pi y_n)N\tau]/N,$$

$$y_{n+1} = y_n, \tag{5}$$

and

$$x_{n+1} = x_n,$$

$$y_{n+1} = y_n + [A_0\cos(2\pi x_n)N\tau]/N, \tag{6}$$

for the first and second half of the period, respectively.

Each advection step is followed by the application—inside each fluid element—of a map on the concentration field, according to

$$C_{n+1}(\mathbf{r}_n) = C_n(\mathbf{r}_n) + \tau S(\mathbf{r}_n) - \tau b C_n(\mathbf{r}_n)^{\gamma}. \tag{7}$$

The indices n in iterations (5)–(7) denote the number of the reaction iteration steps. For the simplicity of the analytical and numerical calculations, we use the same time step τ both for the advection and the reaction map. This is not a limitation, because, as we will see below, the ratio between the characteristic times of the flow and the reaction (given by the

Lyapunov exponents) determines the spatial distribution of the product, and not the ratio between the time steps. During each period of the flow, we apply $M_\tau = 1/\tau$ times the reaction step. Thus for $n(\mathrm{mod}\, M_\tau) \in [0, M_\tau/2)$ we are in the first half period of the flow and we apply the form (5) of the iteration; for $n(\mathrm{mod}\, M_\tau) \in [M_\tau/2, M_\tau)$ we are in the second half period of the flow, and we apply iteration (6), accordingly. Taking $\tau \to 0$ in Eq. (7), we recover the reactive part of Eq. (1) in the time continuous description (see Sec. IV). The reaction and the transport dynamical subsystem is coupled by the space-dependent source term chosen to be $S(\mathbf{r}_n) = a s(\mathbf{r}_n) = a[1 + 0.1 \sin(2\pi x_n)\sin(2\pi y_n)]$, with parameter a representing the strength of the source.

One appealing property of the lattice mixing algorithm is that it opens the possibility to simulate also the effects of the diffusion [17]. In the following calculations, however, we neglect the diffusive transport [18].

In Eq. (7), instead of the two parameters a and b, it is useful to introduce two new nondimensional parameters A and B,

$$A = a/b, \quad B = \tau b, \tag{8}$$

which describe completely the reaction dynamics in the form

$$C_{n+1}(\mathbf{r}_n) = C_n(\mathbf{r}_n) + A\ B\ s(\mathbf{r}_n) - B\ C_n(\mathbf{r}_n)^\gamma. \tag{9}$$

Note, however, that the full advection-reaction problem has a third relevant parameter, too, namely the flow's Lyapunov exponent Λ_F over time τ. The map (9) has a locally homogeneous fixed point at each spatial position: $C^*(\mathbf{r}_n) = [A\ s(\mathbf{r}_n)]^{1/\gamma}$. The stability of these equilibrium states can be characterized by the local reaction Lyapunov exponents $\Lambda_R(\mathbf{r}_n)$, defined by the decay of the linearized transformation around the fixed point,

$$C_{n+1}(\mathbf{r}_n) - C^*(\mathbf{r}_n) = e^{\Lambda_R(\mathbf{r}_n)}[C_n(\mathbf{r}_n) - C^*(\mathbf{r}_n)]. \tag{10}$$

We define the reaction Lyapunov exponent associated to the whole reaction dynamical subsystem as $e^{\Lambda_R} = \langle e^{\Lambda_R(\mathbf{r}_n)} \rangle$, where $\langle * \rangle$ is the spatial average.

In the time continuous case, the Lyapunov exponents are $\lambda_F = 2.7$ for the advection and $\lambda_R = -b$ for the reaction subsystem. The advection and reactive time scales are then given by the inverse of the Lyapunov exponent of the flow and of the reaction rate b, respectively.

The situation is different in the discretized case: the flow's Lyapunov exponent is simply

$$\Lambda_F = \tau \lambda_F. \tag{11}$$

The reaction's characteristic time, however, has a more complex dependence on the reaction rate. Writing the linear reaction iteration step in the form $C_{n+1}(\mathbf{r}_n) = (1-B)C_n(\mathbf{r}_n) + A\ B\ s(\mathbf{r}_n)$, we can see that the reaction Lyapunov exponent in the sense of definition (10) is

$$\Lambda_R = \ln|1 - B|. \tag{12}$$

For a nonlinear decay, it is not possible to analytically calculate the exponent, but we can find an approximate expression by linearizing the reaction iteration step (9) around the fixed point of the reaction,

$$\delta C_{n+1}(\mathbf{r}_n) \simeq \{1 - \gamma B[C^*(\mathbf{r}_n)]^{\gamma-1}\}\delta C_n(\mathbf{r}_n), \tag{13}$$

which can be interpreted as a linear decay equation with a space-dependent effective decay rate $b' = \gamma B[C^*(\mathbf{r}_n)]^{\gamma-1}$, approximated by the spatial average $\gamma B(C^*)^{\gamma-1}$. The reaction Lyapunov exponent is then

$$\Lambda_R \simeq \ln|1 - \gamma B(C^*)^{\gamma-1}| \tag{14}$$

$$= \ln|1 - \gamma B(A)^{1-1/\gamma}|, \tag{15}$$

since the average of $s(\mathbf{r})$ is unity. As we will see below, this expression gives a good approximation of the numerical findings. We study the case when Λ_R is negative, i.e., the parameter range (for linear decay $0 < B < 1$, for quadratic decay $0 < B < 1/C^*$) where the reaction's fixed point is stable and the concentrations converge to the equilibrium value given by this fixed point.

IV. SMOOTH-FILAMENTAL TRANSITIONS

After a short transient time, a steady state sets in the system, in which the spatial distribution of the concentration field can be smooth or filamental. The "roughness" of the concentration field results from the competition between the dissipative stable reaction dynamics (that tends to relax to the smooth equilibrium distribution and thus reduces concentration fluctuations) and the dispersion due to chaotic mixing (which, by stretching and folding fluid elements, enhances the spatial gradients of the concentrations) [11,13,14]. When the two effects become balanced, a smooth-filamental transition takes place in the system.

For a quantitative characterization of the reactive field $C_{n+1}(\mathbf{r}_n)$, we use the Hölder exponent α, given by the scaling of the concentration differences between two spatially close (at distance $\delta\mathbf{r}_n$) points,

$$|\delta C(\delta\mathbf{r}_n)| \equiv |C_{n+1}(\mathbf{r}_n + \delta\mathbf{r}_n) - C_{n+1}(\mathbf{r}_n)| \sim |\delta\mathbf{r}_n|^{\alpha(\mathbf{r_n})}. \tag{16}$$

For simplicity, we assume a uniform Hölder exponent $\alpha(\mathbf{r}) = \alpha$ in each spatial point (mono-affine approach). A filamental structure presents anomalous scaling $\alpha < 1$, while a smooth function has $\alpha = 1$. For the linear case, the Hölder exponent can be exactly calculated (see the Appendix for the detailed algebra) as

$$\alpha = \min\left\{\frac{-\ln(1-B)}{\Lambda_F}, 1\right\} \tag{17}$$

$$= \min\left\{\frac{|\Lambda_R|}{\Lambda_F}, 1\right\}, \tag{18}$$

showing that the smooth-filamental transition ($\alpha = 1$) takes place when the Lyapunov exponents of the reaction and advection dynamics are equal in absolute value. In the case of the second-order decay, using Eq. (18), we can write an approximant for the Hölder exponent as

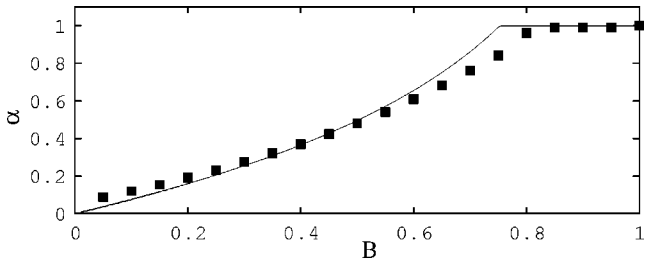

FIG. 1. Variation of the Hölder exponent with the dimensionless reaction rate B, in the case of a linearly decaying substance for $A=0.5$, $\Lambda_F=1.35$. The squares represent the numerically measured values, while the continuous line is the theoretically predicted result Eq. (17). The critical value of the decay rate for which the smooth-filamental transition takes place from Eq. (17) is $B_c=1-\exp(-\Lambda_F)=0.74$.

$$\alpha = \min\left\{\frac{-\ln|1-2B\sqrt{A}|}{\Lambda_F},1\right\}. \tag{19}$$

In general, the Hölder exponent can be approximated as

$$\alpha = \min\left\{\frac{-\ln|1-\gamma\, B\, A^{1-1/\gamma}|}{\Lambda_F},1\right\}. \tag{20}$$

We can see that for the linear decay, the roughness of the concentration distributions depends only on one of the dimensionless parameters, on B. For higher-order reactions, the expression of the Hölder exponent also contains the parameter A.

In order to investigate numerically the effects of the competition between advection and reaction, we keep constant the parameters of the flow and vary that of the source and reaction A and B.

(i) In the case of linear decay, first we numerically measured the Hölder exponents of the different concentration distributions (Fig. 1), for constant parameters $\Lambda_F=1.35$, $\tau=1/2$, and changing B. We also kept the parameter $A=0.5$ constant because the roughness does not depend on it in this case.

The distributions corresponding to small decay rates show filamental structures. Increasing the decay rate, the roughness decreases to the point where the phase transition between the filamental and smooth distributions takes place ($B_c=0.74$). At larger values of the decay rate, due to the dominant effect of the reaction, the final distribution becomes smooth. The Hölder exponent depends logarithmically on the strength B of the reaction, instead of linearly, as was shown in the time continuous approach [13,14].

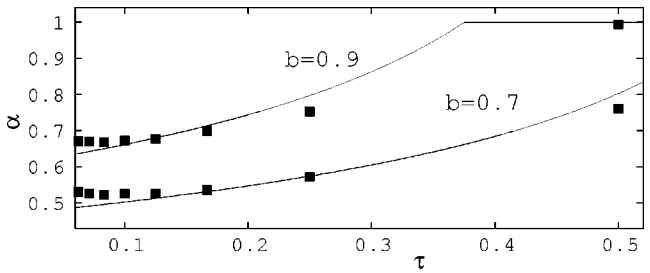

FIG. 2. Variation of the Hölder exponent as a function of the time lag ($\tau=1/2,1/4,1/6\ldots,1/16$) of the map in the case of a linear decay ($a=0.5b$, $\lambda_F=2.7$). The squares represent the numerically measured values, while the continuous line is the theoretically predicted result Eq. (17). The deviations from the theoretical result for small τ are due to the effects of the numerical diffusion (proportional to $1/\tau$).

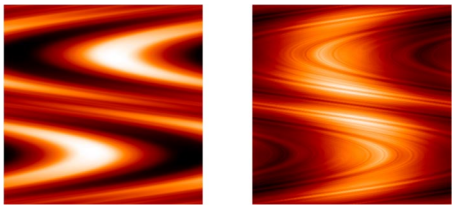

FIG. 3. Snapshot on the (x,y) plane of the concentration pattern of the linearly decaying substance under the chaotic flow, for time step $\tau=1/2$ and $\tau=1/8$ ($a=0.5b$, $b=0.9$, $\lambda_F=2.7$). Darker levels indicate smaller concentrations.

Since the discretization of the processes due to the different lifetime of the species has special importance, we varied the time step τ by keeping all the other parameters (a, b, and λ_F) fixed. The change is more drastic in this case (see Fig. 2). For instance, by applying twice the linear reaction step during one period of the flow ($M_\tau=2;\tau=0.5$) at $b=0.9$, the resulting steady-state distribution is smooth. By increasing the number of reaction steps M_τ during one period (reducing τ), filamental structure appears in the steady state (Figs. 3 and 4). This means that in exactly similar circumstances, the different lifetime of the species can result in different spatial distributions of the population, or in other words the difference in the species' lifetime can induce smooth-filamental phase transition.

(ii) In the case of quadratic decay, for the same parameters as for the linear decay $\Lambda_F=1.35$, $\tau=1/2$, $A=0.5$, we find a different scenario. The major change in the dynamics is the appearance of a reentrance transition (Figs. 5–8), nonexistent in the time continuous description. Surprisingly, the filamental structure disappears and later reappears.

For a better visualization, we show in Fig. 5 snapshots on the chemical pattern for increasing reaction rates, displaying clearly the different spatial structures. Interestingly, above the second transition point the roughness of the field increases as the decay rate B is increased further. To demonstrate the general character of the phenomenon we show the variation of the Hölder exponent together with the two transition points for the cases when $A=0.5=\text{const}$ (a is proportional to b) in Fig. 7 and when both A and B are changed but $A=2/B$ ($a=\text{const}$) in Fig. 8. The filamental structure always

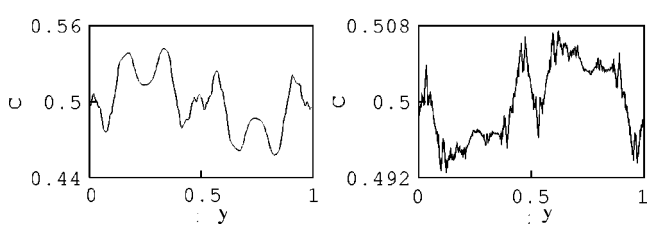

FIG. 4. Transversal cuts on the patterns shown in Fig. 3 along the $x=0.25$ line for time steps $\tau=1/2$ (left) and $\tau=1/8$ (right).

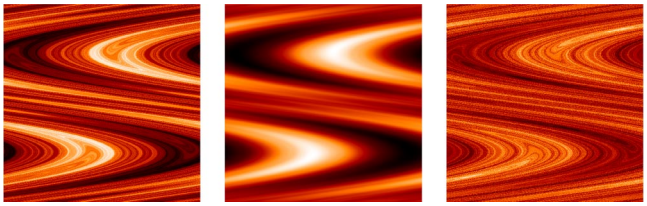

FIG. 5. Snapshots on the (x,y) plane of the concentration pattern of the quadratically decaying substance under the chaotic flow, for decay rate $B=0.04$, $B=0.3$, $B=0.8$ from left to right. Darker levels indicate smaller concentrations ($A=2/B$, $\Lambda_F=1.35$).

reappears.

The condition for the phase transitions ($\alpha=1$) in the map yields from Eq. (19) the critical values

$$B_{c\pm}=\frac{1\pm e^{-\Lambda_F}}{2\sqrt{A}}. \tag{21}$$

Since the Hölder exponent α depends implicitly (by B) on the time lag τ of the map, the lifetime of the species has a considerable impact on the dynamics also in the case of a quadratic reaction. Instead of the simple phase transition found in the case of linear decay, relation (19) shows that now, for increasing values of the time step, a reentrance transition is present in the dynamics.

V. THE TIME CONTINUOUS LIMIT

Our results derived for maps go into those of Refs. [13,14] determined for the time continuous approach of the linear decay problem. The continuous-time limit can be performed by taking $B\to 0$ and $\tau\to 0$ in the difference equation over the time lag τ, with the conditions $B/\tau\to b$. The Hölder exponent (18) derived for the linear decay in the map (when $|\Lambda_R|<\Lambda_F$, i.e., $\alpha<1$) goes in the time continuous limit $\tau\to 0$ in

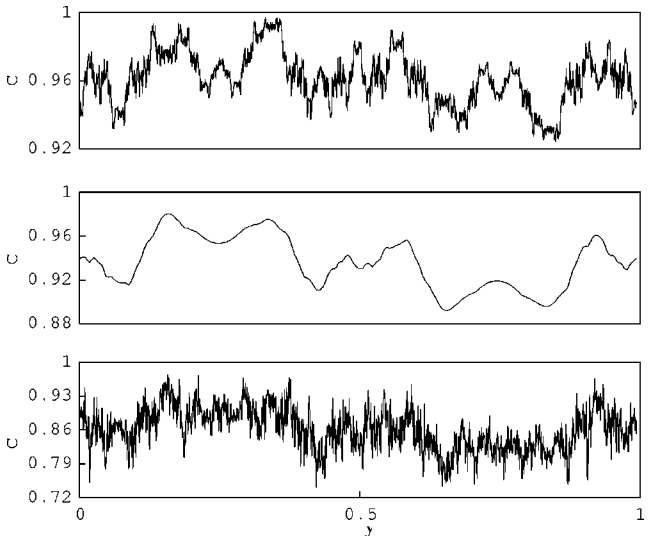

FIG. 6. Transversal cuts on the patterns shown in Fig. 5 along the $x=0.25$ line for decay rates $B=0.04$, $B=0.3$, $B=0.8$ (from top to bottom).

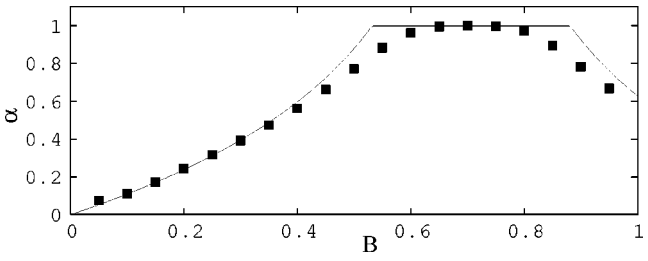

FIG. 7. Variation of the Hölder exponent as a function of the reaction rate B for quadratic decay and $A=0.5$, $\Lambda_F=1.35$. The squares represent the numerically measured values, while the continuous line is the theoretically predicted curve Eq. (19).

$$\alpha=\frac{-\ln|1-B|}{\Lambda_F}\simeq\frac{B}{\lambda_F\tau}\to\frac{b}{\lambda_F}, \tag{22}$$

where $\lambda_F=\Lambda_F/\tau$ [see Eq. (11)]. For $|\Lambda_R|>\Lambda_F$, the Hölder exponent remains $\alpha=1$, unchanged, representing a smooth concentration distribution.

For quadratic decay, Eq. (19) gives the Hölder exponent (considering the $|\Lambda_R|<\Lambda_F$ case for small τ) [21],

$$\alpha=\frac{-\ln|1-2B\sqrt{A}|}{\Lambda_F}\to\frac{2\sqrt{ab}}{\lambda_F}. \tag{23}$$

The critical values of the continuous-time reaction rates $b_c\equiv B/\tau$ for $\tau\ll 1$ from Eq. (21) are

$$b_{c\pm}=\frac{1\pm[(1-\lambda_F\tau)]^2}{4\tau^2 a}. \tag{24}$$

We observe that b_{c-} possesses a finite limit $b_{c-}=\lambda_F^2/4a$, showing where the phase transition takes place in the continuous-time description, while b_{c+} diverges as $1/\tau^2$ in the $\tau\to 0$ limit, indicating that the second phase transition disappears (is shifted to $b_{c+}=\infty$ in the time continuous limit).

VI. GENERALIZATION

The second phase transition and the reappearance of the filamental phase are characteristic not only of our studied case, but of a wider class of reactions. Note that for $\gamma=2$, without a source term, recurrence (7) approaches in the limit $B=1$ the logistic map $C_{n+1}=rC_n(1-C_n)$ with $r=1$ (dotted line in Fig. 9). The logistic map is a well known, classical example for the description of population dynamics in cases when the growth of the population is stopped by some lim-

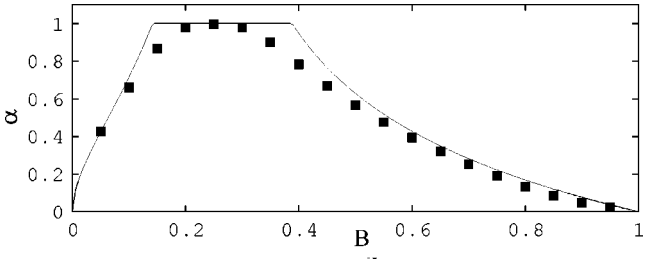

FIG. 8. The same as Fig. 7 but for $A=2/B$.

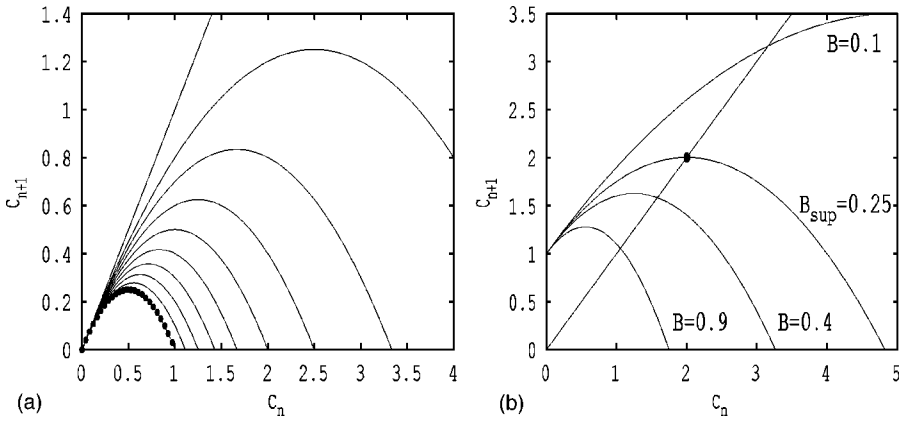

FIG. 9. Behavior of recurrence (7) for reactions with different parameter B with (a) and without (b) source term. For increasing B ($B=0.2,0.3,0.4,0.5,0.6,0.7,0.8,0.9$) we approach the dotted line (a) representing the logistic map that we can obtain in the limit $B=1$. The straight line is the diagonal $C_{n+1}=C_n$.

iting factors (competition for sources, food, or light).

We will show that the appearance of the second transition point is caused by the fact that the recurrence (7) describing the reaction is a nonmonotonous function for $\gamma>1$. In the following calculation, instead of the function $f_B(C_n)=C_n(1-B\,C_n)$, we use a general $f_B(C_n)$ function with a smooth maximum and a slope less than 1 in the origin. Without a source term, the equation describing the reaction has only one fixed point in the origin, according to the fact that a decaying reaction without a source leads to a vanishing population. We assure a nontrivial concentration distribution in the steady state by introducing a source term in the equation. For the sake of simplicity, we consider, without loss of generality, the case $\langle ABs\rangle=1$ (for other $\langle ABs\rangle$ values, only a simple shift along the y axes is needed). Thus

$$C_{n+1}=1+f_B(C_n). \tag{25}$$

The fixed point of the map is given by its intersection with the diagonal (Fig. 9) $C^*=1+f_B(C^*)$. The map linearized around the fixed point is

$$\delta C_{n+1}=\left.\frac{\partial f_B(C_n)}{\partial C_n}\right|_{C_n=C^*}\delta C_n. \tag{26}$$

The reaction Lyapunov exponent Λ_R appearing in expression (18), according to definition (10) and to Eq. (26), is

$$\Lambda_R=\ln\left|\left.\frac{\partial f_B(C_n)}{\partial C_n}\right|_{C_n=C^*}\right|, \tag{27}$$

which contains the slope of the function $f_B(C_n)$ in the fixed point. Therefore, the roughness of the concentration distribution is determined by the absolute value of this gradient. From Eq. (27) it is clear that the character of the concentration distribution does not depend on the *strength* of the reaction, as it was intuitively expected, but rather on the *stability* of the reaction.

For a certain value of the dimensionless reaction rate B, B_{sup}, the diagonal intersects the map in its maximum point. For B_{sup}, the fixed point of the reaction is superstable, i.e., the reaction Lyapunov exponent is infinite. This B_{sup} value is given by the condition

$$\left.\frac{\partial f_B(C_n)}{\partial C_n}\right|_{B=B_{sup},C_n=C^*}=0, \tag{28}$$

which in the cases shown in Fig. 7 and 8 are $B_{sup}=\sqrt{2}/2$ and $B_{sup}=0.25$, respectively. Since for the values B_{sup} corresponding to the superstable fixed point $\Lambda_R=-\infty$, cf. Eq. (18), the Hölder exponent has a "virtual singularity" [20]. Increasing the reaction rate above this value, the stability of the reaction decreases to smaller and smaller values, until it balances the stability of the advection when a phase transition takes place in the system. For larger values of the reaction rate, the effects of the advection will dominate the effects of the reaction and a filamental structure will reappear in the system.

More visually [see Fig. 9(b)] for any $B<B_{sup}$, the diagonal intersects the function in points with positive gradient. For $B>B_{sup}$, the slope in the fixed point sweeps over the same values but with negative sign. Thus for each $B'<B_{sup}$ value of the parameter we can find a certain $B''>B_{sup}$ counterpart for which in the fixed point the functions have equal slopes in absolute value. The corresponding Lyapunov exponents are equal, and the roughness of the field is the same, accordingly. Thus the filamental phase reappears for increasing values of the parameter. Even though the reaction is becoming stronger, the stability of the reaction is what determines the spatial structure of the concentration field.

In general, this implies that for every smooth function $f_B(C_n)$ with one maximum point, a second phase transition appears in the system independently from any additional assumption on the character of the reaction.

VII. DISCUSSION AND CONCLUSION

We have investigated the interplay between mixing and reaction, by focusing on the effects introduced by a discrete map description, in comparison with the time continuous approach of the problem. For first-order reactions, we found only a quantitative change in comparison with the continuous case: the dependence of the roughness on the reaction rate is logarithmic and not linear, but the fact that a stronger reaction smooths out the structure remains unchanged.

For second-order reactions, however, a second transition point appears. For increasing decay rates, the filaments dis-

appear at the beginning, but upon increasing further the reaction strength, they reappear. Surprisingly, the faster reaction is not able to smooth out the structure of the concentration field, as expected. In conclusion, it is not the strength but rather the stability of the reaction that determines the roughness of the chemical pattern. This stability depends on the time step of the map. Thus only the different time step of the map (different lifetime of the species) can modify drastically the dynamics (changes on the scaling properties, Hölder exponents, power spectrum), to the point when it produces a phase transition in the system.

Based on the generalization presented in the preceding section, we suggest that the reappearance of the filamental structure is a generic property of systems in which the reaction map is smooth, nonmonotonous, and with a maximum point in the studied domain. An extension to the logistic map, as shown before, is straightforward, pointing out the relevance of the findings to biological populations dynamics.

The qualitative difference between the cases of linear and nonlinear reactions is an argument against the statement that a linear decay can be considered as an approximation to more complex chemical or biological evolutions with stable chemical dynamics. Within the framework of a discrete time dynamics, this statement is no longer valid.

As an extension of the present work to more realistic situations of biological origin, we would suggest similar investigations of a model with a periodically changing reaction rate in Eq. (1), describing a situation in which for half of a period the reaction goes on and for half of a period it is stopped. This model, which will be the subject of further investigations, represents a transition between the merely continuous description and the pure discrete representation of the dynamics.

ACKNOWLEDGMENTS

I would like to thank Z. Neufeld and T. Tél both for encouragement and for enlightening conversations. Their continuous support led to a considerable improvement of the work. Special thanks go to I. Scheuring for the biological background of the physical problem. I am grateful for the suggestions of E. Hernandez Garcia. I am also indebted to H. Kantz for his illuminating ideas and to E. G. Altmann for a careful reading of the paper. The support of the Hungarian Science Foundation (OTKA, No. TS044839) is acknowledged.

APPENDIX: THE HÖLDER EXPONENT

For the evaluation of the Hölder exponent, we need the difference $\delta C_{n+1}(\delta \mathbf{r}_n) = C_{n+1}(\mathbf{r}_n + \delta \mathbf{r}_n) - C_{n+1}(\mathbf{r}_n)$ at time $t_n = n\tau$ of the value of the chemical field at two different points separated by a small distance $\delta \mathbf{r}_n$. This difference can be obtained by following two trajectories ending at preselected points $\mathbf{r}_n + \delta \mathbf{r}_n$ and $\mathbf{r}_n$ after the nth advection step, and taking into account their history, i.e., the temporal evolution of the chemical field along these trajectories from a previous kth reaction iteration step.

Applying the reaction iteration from the initial C_0 values to C_1, we obtain after the first reaction step $C_1(\mathbf{r}_0) = (1 - B)C_0(\mathbf{r}_0) + ABs(\mathbf{r}_0)$, which in the same time period is advected by flow to the next position $\mathbf{r}_1$: $C_1(\mathbf{r}_0) = C_1(\mathbf{r}_1)$. After the nth reaction step, the concentration will be

$$C_{n+1}(\mathbf{r}_n) = (1 - B)^{n+1} C_0(\mathbf{r}_0) + \sum_{k=0}^{n} ABs(\mathbf{r}_k)(1 - B)^{n-k}. \tag{A1}$$

This expression contains (a) the remnant of the initial concentration in the starting points of the trajectory, which decays as time goes on, and (b) the sum of the source contributions accumulated in the points visited by these trajectories in the last $n-k$ steps. The first term on the right-hand side containing the initial values of the concentration field tends to zero in the limit $n \to \infty$. Evaluating the difference $\delta C_{n+1}(\delta \mathbf{r}_n)$ with expression (A1), after neglecting the first term on the right-hand side, we obtain

$$\delta C_{n+1}(\delta \mathbf{r}_n) = \sum_{k=0}^{n} \delta s(\mathbf{r}_k, \delta \mathbf{r}_k) AB(1 - B)^{n-k}, \tag{A2}$$

where $\delta \mathbf{r}_k$ with $(0 < k < n)$ is the time-dependent (more exactly step-dependent) distance between the two trajectories and δs is the difference of the source term at points $\mathbf{r}_k$ and $\mathbf{r}_k + \delta \mathbf{r}_k$. The time dependence of the distances $|\delta \mathbf{r}_k|$ in Eq. (A2) can be estimated by considering the time-reversed advection steps starting from $\delta \mathbf{r}_n$ at t_n, as $|\delta \mathbf{r}_k| = |\delta \mathbf{r}_n| e^{\Lambda_F (n-k)}$, where $k < n$ for almost all orientations $\mathbf{n}_n = \delta \mathbf{r}_n / |\delta \mathbf{r}_n|$, except the ones parallel to the local unstable direction.

By taking the limit $\delta \mathbf{r}_n \to 0$ and expanding $\delta s(\mathbf{r}_k, \delta \mathbf{r}_k)$ to linear order in $\delta \mathbf{r}_k$, we obtain

$$\frac{\delta C_{n+1}(\delta \mathbf{r}_n)}{|\delta \mathbf{r}_n|} = \sum_{k=0}^{n} \nabla s(\mathbf{r}_k) \mathbf{n}_k AB(1 - B)^{n-k} e^{\Lambda_F (n-k)}. \tag{A3}$$

The filamental or smooth structure of the concentration field depends on the convergence of the sum appearing on the right-hand side. Using $(1-B)^{n-k} \equiv e^{(n-k)\ln(1-B)}$, and rewriting $\delta \mathbf{r}_n = \mathbf{n}_n |\delta \mathbf{r}_n|$, the concentration gradient ∇C along the direction of $\mathbf{n}_n$ can be written as a sum of exponential terms,

$$\mathbf{n}_n \nabla C_{n+1}(\mathbf{r}_n) = \sum_{k=0}^{n} \nabla s(\mathbf{r}_k) \mathbf{n}_k AB e^{[\Lambda_F + \ln(1-B)](n-k)}, \tag{A4}$$

which is convergent if the exponents are negative. Taking into account the form of the reaction Lyapunov exponent, we can see that for $\Lambda_F < |\Lambda_C|$ the sum remains finite and the corresponding concentration field (when $n \to \infty$) is smooth (differentiable). For $\Lambda_F > |\Lambda_C|$, the derivatives of C_{n+1} diverge, resulting in an almost nowhere differentiable field, thus the field has a filamental character.

The Hölder exponent results from the scaling properties of $\delta C_{n+1}(\delta \mathbf{r}_n)$. In the case of $\Lambda_F < |\Lambda_C|$, in the $\mathbf{r}_n \to \mathbf{0}$ limit we find in Eq. (A3) the simple scaling

$$\delta C_{n+1}(\delta \mathbf{r}_n) \sim |\delta \mathbf{r}_n|. \tag{A5}$$

Thus the Hölder exponent, cf. Eq. (16), is $\alpha=1$. When $\Lambda_F < |\Lambda_C|$, the behavior of the divergent sum is governed by the term corresponding to $k=0$, thus we obtain

$$\delta C_{n+1}(\delta \mathbf{r}_n) \sim |\delta \mathbf{r}_n| e^{[\Lambda_F + \ln(1-B)]n}. \tag{A6}$$

Inserting $n=\Lambda_F^{-1}\ln(|\delta \mathbf{r}_0|/|\delta \mathbf{r}_n|)$ in Eq. (A6), we find that the concentration field scales as

$$\delta C_{n+1}(\mathbf{r}_n, \delta \mathbf{r}_n) \sim |\delta \mathbf{r}_n|^{-\Lambda_C/\Lambda_F}. \tag{A7}$$

This corresponds to the Hölder exponent $\alpha=|\Lambda_C|/\Lambda_F$.

[1] P. H. Haynes, Transport, Stirring and Mixing in the Atmosphere, in *Mixing: Chaos and Turbulence*, edited by H. Chaté and E. Villermaux (Kluwer, Dordrecht 1999).

[2] R. P. Wayne, *Chemistry of Atmospheres* (Oxford University Press, Oxford, 2000).

[3] K. H. Mann and J. R. N. Lazier, *Dynamics of Marine Ecosystems. Biological-physical Interactions in the Oceans* (Blackwell Scientific Publications, Boston, 1991).

[4] A. Bracco, A. Provenzale, and I. Scheuring, Proc. R. Soc. London, Ser. B **267**, 1795 (2000).

[5] J. M. Ottino, *The kinematics of Mixing: Stretching, Chaos and Transport* (Cambridge University Press, Cambridge, 1989).

[6] T. Tél, T. Nishikawa, A. E. Motter, C. Grebogi, and Z. Toroczkai, Chaos **14**, 72 (2004).

[7] Gy. Károlyi, Á. Péntek, I. Scheuring, T. Tél, and Z. Toroczkai, PNAS **97**, 13 661 (2000).

[8] Gy. Károlyi, Á. Péntek, Z. Toroczkai, T. Tél, and C. Grebogi, Phys. Rev. E **59**, 5468 (1999).

[9] Z. Toroczkai, Gy. Károlyi, Á. Péntek, T. Tél, and C. Grebogi, Phys. Rev. Lett. **80**, 500 (1998).

[10] J. M. Cushing *et al., Chaos in Ecology: Experimental Nonlinear Dynamics* (Academic Press, New York, 2003).

[11] E. Hernandez-Garcia, C. Lopez, and Z. Neufeld, *Chaos in Geophysical Flows*, edited by G. Bofetta, G. Lacorata, G. Visconti, and A. Vulpiani (OTTO Editore, Torino, 2003).

[12] C. Lopez, E. Hernandez-Garcia, O. Piro, A. Vulpiani, and E. Zambianchi, Chaos **11**, 397 (2001).

[13] Z. Neufeld, C. López, and P. H. Haynes, Phys. Rev. Lett. **82**, 2606 (1999).

[14] Z. Neufeld, C. Lopez, E. Hernandez-Garcia, and T. Tél, Phys. Rev. E **61**, 3857 (2000).

[15] E. R. Abraham and M. M. Bowen, Chaos **12**, 373 (2002).

[16] R. E. Lee, *Phycology*, 3rd ed. (Cambridge University Press, Cambridge, UK, 1999).

[17] R. T. Pierrehumbert, Chaos **10**, 61 (2000).

[18] The diffusion coefficient is $D=D_{map}\Delta x^2/\tau$ with D_{map} the diffusion coefficient in the lattice mixing algorithm. We used $D_{map}=0.01$, $\Delta x=1/4000$, and $\tau \in \{1/2, 1/30\}$, which give the value $D \in \{10^{-7}, 10^{-8}\}$.

[19] R. T. Pierrehumbert, Chaos Sol. Fract. **4**, 1091 (1994).

[20] The ratio of the two Lyapunov exponents has a singularity in the superstable fixed point of the dynamics.

[21] The time continuous quadratic reaction $\dot{C}=S-bC^2$ leads to the Lyapunov exponent $\lambda_R=2bC^*_{cont}$, where the fixed point is given by $C^*_{cont} \approx \sqrt{a\langle s(\mathbf{r}_n)\rangle/b}=\sqrt{a/b}$.